Available online at www.sciencedirect.com
ScienceDirect
Energy Conversion and Management 48 (2007) 3120–3134
ENERGY CONVERSION & MANAGEMENT
www.elsevier.com/locate/enconman

Switching EKF technique for rotor and stator resistance estimation in speed sensorless control of IMs

Murat Barut [a], Seta Bogosyan [a,*], Metin Gokasan [b]

[a] University of Alaska Fairbanks, Department of Electrical and Computer Engineering, Fairbanks, AK 99775, USA
[b] Istanbul Technical University, Electrical and Electronic Engineering Faculty, 34390 Istanbul, Turkey

Received 10 December 2005; received in revised form 21 September 2006; accepted 29 April 2007
Available online 25 September 2007

Abstract

High performance speed sensorless control of induction motors (IMs) calls for estimation and control schemes that offer solutions to parameter uncertainties as well as to difficulties involved with accurate flux/velocity estimation at very low and zero speed. In this study, a new EKF based estimation algorithm is proposed for the solution of both problems and is applied in combination with speed sensorless direct vector control (DVC). The technique is based on the consecutive execution of two EKF algorithms, by switching from one algorithm to another at every n sampling periods. The number of sampling periods, n, is determined based on the desired system performance. The switching EKF approach, thus applied, provides an accurate estimation of an increased number of parameters than would be possible with a single EKF algorithm. The simultaneous and accurate estimation of rotor, R'_r and stator, R_s resistances, both in the transient and steady state, is an important challenge in speed sensorless IM control and reported studies achieving satisfactory results are few, if any. With the proposed technique in this study, the sensorless estimation of R'_r and R_s is achieved in transient and steady state and in both high and low speed operation while also estimating the unknown load torque, velocity, flux and current components. The performance demonstrated by the simulation results at zero speed, as well as at low and high speed operation is very promising when compared with individual EKF algorithms performing either R'_r or R_s estimation or with the few other approaches taken in past studies, which require either signal injection and/or a change of algorithms based on the speed range. The results also motivate utilization of the technique for multiple parameter estimation in a variety of control methods.

Keywords: Induction motor; Extended Kalman filter with switching; Sensorless control; Load torque; Rotor and stator resistance estimation; Zero speed operation

1. Introduction

Industry workhorse induction motors (IMs) constitute a theoretically interesting and practically important class of nonlinear systems and, hence, a benchmark problem for nonlinear control [1]. IMs enjoy several inherent advantages, like simplicity, reliability, low cost and almost maintenance free electrical drives [2]; however, the speed sensorless high performance control of IMs currently continues being a challenge due to the highly coupled nonlinearities and multi-input, multi-output nature of the motor model. The problem has been addressed by a variety of methods such as, *field-oriented control* (FOC) or *vector control* [3], *direct torque control* (DTC) [4], *input–output linearization (feedback linearization) controller* [3,5], *sliding mode control* (SMC) [6] and *passivity-based control* (PBC) [3], each of which aims at independent control of the torque and flux. Additional difficulties are due to unknown load disturbances and parameter uncertainties, mostly related to the stator and rotor resistances varying with operating conditions.

* Corresponding author. Tel.: +1 907 474 2755; fax: +1 907 474 5135.
E-mail address: s.bogosyan@ual.edu (S. Bogosyan).

0196-8904/$ - see front matter © 2007 Published by Elsevier Ltd.
doi:10.1016/j.enconman.2007.04.026

There are also well known problems related to high performance control, particularly in the very low/zero speed region, mainly due to lost rotor information on the stator side as well as noise and signal acquisition errors [1,7,8]. In this regard, it is essential to design estimation and control methods that provide robustness, predominantly against the variations of R_s, R'_r and t_L while also providing solutions to problems at and around zero speed.

Some recent studies seeking an observer based solution to the problem of parameter variations can be listed as follows; in Ref. [9], beside a speed estimator, a sliding mode based flux observer and an online sliding mode adaptation for the stator resistance is designed for DTC of the IM, but the speed estimator and the resistance adaptation suffer from variations of the rotor resistance and the load torque, respectively. In the speed sensorless study based on a speed adaptive flux observer [10], the stator resistance has been estimated based on a two time scale approach, while in the extended Luenberger observer (ELO) in Ref. [11], the rotor fluxes and rotor velocity are estimated, as well as step type load torque; however, no estimation has been conducted for the stator resistance. Also, neither of the studies in Refs. [10,11] have taken the rotor resistance into consideration. On the other hand in Ref. [12], the angular velocity and slip frequency, ω_r (reflecting the effect of the load torque) have been taken into account in addition to the rotor resistance only with an initial value of $R'_r(0) = 0.85R'_{rn}$.

There are also extended Kalman filter (EKF) applications in the literature for the control of IMs with velocity sensors [13–15] and without sensors. Different from the other methods, the model uncertainties and nonlinearities inherent in IMs are well suited to the stochastic nature of EKFs [16]. With this method, it is possible to make an online estimation of states while performing simultaneous identification of parameters in a relatively short time interval [17–19] by also taking system/process and measurement noises directly into account. This is the reason why the EKF has found wide application in sensorless control of IM's in spite of its computational complexity. Among recent sensorless studies using EKF estimation for IMs, Refs. [20,21] estimate the flux and velocity, while Ref. [22] uses an adaptive flux observer in combination with a second order Kalman filter for the same purpose. None of these studies estimate the load and motor resistances, resulting in a performance that is sensitive to the variation of these parameters. In Refs. [23–25], the velocity is estimated as a constant parameter, which gives rise to a significant estimation error in the velocity during the transient state, especially under instantaneous load variations, although the performance is improved in the steady state. While Refs. [23,24] are sensitive to rotor resistance variations, Ref. [25] also estimates the rotor resistance. However, the estimation of rotor resistance is performed by the injection of low amplitude, high frequency signals to the flux reference in the DVC of IMs. This has caused fluctuations in the motor flux, torque and speed. Finally, recent studies of the authors [26,27] estimating the velocity via consideration of the equation of motion in the EKF model, together with the estimation of rotor resistance and mechanical uncertainties, demonstrate improved results. However, the results are sensitive to variations of stator resistance, indicating the necessity of an approach that estimates rotor resistance and stator resistance simultaneously and accurately besides the load torque for high performance control in a wide operation range, including very low/zero speed.

Among the studies reported so far on R_s and R'_r estimation, Ref. [12] states that simultaneous estimation of the stator and rotor resistances gives rise to instability in the speed sensorless case. On the other hand, in studies such as Refs. [28,29], the stator and rotor resistances are estimated by injecting high frequency signals to the flux and magnetizing current commands while also estimating the speed and rotor flux. However, in Ref. [28], the algorithm identifying the resistances used in the feedback linearization controller is applicable only when the sensorless speed control system is in steady state but not when the load torque is varying largely or when the speed command is being changed, as stated by the authors. On the other hand, in Ref. [29], it is stated that persistent operation at zero frequency is not possible and that the proposed drive can compete with a speed sensor equipped drive only if accuracy in steady state is not essential and operation under high loads is not a requirement; Ref. [30] presents a model reference adaptive system (MRAS) based on three models of which one is used for estimation of the rotor time constant via high frequency signal injection. The other two models are used interchangeably by enabling the stator resistance estimation only during short intervals during which the rotor speed has reached steady state. As for the remaining few studies performing R_s and R'_r estimation, as in Refs. [31–33], R'_r estimation is conducted only by adjusting its value in proportion to the estimated R_s.

The major contribution of this study is the development of a novel EKF based estimation technique, which aims at accurate estimation of an increased number of parameters, both in the transient and steady state, for sensorless IM control. The technique does not require signal injection and/or algorithm changes for different parameters or speed ranges, as is commonly practised in similar past studies. It is based on two EKF algorithms that are switched *on* and *off* every n sampling periods, the output parameters and states of which are used in the direct vector control (DVC) of IMs With this algorithm in this study, accurate estimation of both R_s and R'_r is achieved, as a novelty in sensorless control of IMs, together with the unknown load torque, velocity, flux and current components. Simulation results are presented using the new algorithm for the DVC of IMs with the switching period taken as $100 \times T$ for the desired transient and steady state performance. The results highlight the significant improvement achieved with the

simultaneous estimation of R_s and R'_r over EKF results obtained by either R_s or R'_r estimation only.

This paper is organized as follows; after the Introduction in Section 1, Section 2 gives the extended mathematical models considered at each step of the EKF estimation. Next, Section 3 describes the development of the EKF algorithm, followed by Section 4 presenting a brief description of the direct vector control (DVC) scheme. The performance of the proposed approach is tested by simulations with the results presented in Section 5 and finally, Conclusions are listed in Section 6.

2. Extended mathematical models of the IM

The sensorless DVC scheme developed for IMs requires estimation of the stator flux components, $\psi_{r\alpha}$, $\psi_{r\beta}$, angular velocity, ω_m and stator current components $i_{s\alpha}$ and $i_{s\beta}$, which are also measured as output. In this study, two extended models are developed, one that includes the rotor resistance, R'_r and the other the stator resistance, R_s. The rest of the variables are the same for both extended vectors, $\underline{x}_{ei}$, used in the two EKF algorithms that run consecutively. The extended models can be given (as referred to the stator stationary frame) in the following general form:

$$\begin{aligned}\dot{\underline{x}}_{ei}(t) &= \underline{f}_{ei}(\underline{x}_{ei}(t), \underline{u}_e(t)) + \underline{w}_{i1}(t)\\ &= \underline{A}_{ei}(\underline{x}_{ei}(t))\underline{x}_{ei}(t) + \underline{B}_e\underline{u}_e(t) + \underline{w}_{i1}(t) \qquad (1)\\ \underline{Z}(t) &= \underline{h}_{ei}(\underline{x}_{ei}(t)) + \underline{w}_{i2}(t) \quad \text{(measurement equation)}\\ &= \underline{H}_e\underline{x}_{ei}(t) + \underline{w}_{i2}(t) \qquad (2)\end{aligned}$$

Here, $i = 1, 2$; the extended state vector $\underline{x}_{ei}$ represents the estimated states and load torque, t_L, which is included in the extended state vector as a constant state with the assumption of a slow variation with time; $\underline{f}_{ei}$ is a nonlinear function of the states and inputs; $\underline{A}_{ei}$ is the system matrix; $\underline{u}_e$ is a control input vector; $\underline{B}_e$ is the input matrix; $\underline{w}_{i1}$ is process noise; $\underline{h}_{ei}$ is a function of the outputs; $\underline{H}_e$ is the measurement matrix; and $\underline{w}_{i2}$ is measurement noise. Based on the general form in Eqs. (1) and (2), the detailed matrix representation of the two IM models can be given as below:

Model 1: Extended model of IM derived for the estimation of R_s, (Model-R_s):

$$\underbrace{\begin{bmatrix}\dot{i}_{s\alpha}\\ \dot{i}_{s\beta}\\ \dot{\psi}_{r\alpha}\\ \dot{\psi}_{r\beta}\\ \dot{\omega}_m\\ \dot{t}_L\\ \dot{R}_s\end{bmatrix}}_{\dot{\underline{x}}_{e1}} = \underbrace{\begin{bmatrix} -\left(\frac{R_s}{L_\sigma}+\frac{L_m^2R'_r}{L_\sigma L'^2_r}\right) & 0 & \frac{L_mR'_r}{L_\sigma L'^2_r} & \frac{L_m}{L_\sigma L'_r}p_p\omega_m & 0 & 0 & 0\\ 0 & -\left(\frac{R_s}{L_\sigma}+\frac{L_m^2R'_r}{L_\sigma L'^2_r}\right) & -\frac{L_m}{L_\sigma L'_r}p_p\omega_m & \frac{L_mR'_r}{L_\sigma L'^2_r} & 0 & 0 & 0\\ L_m\frac{R'_r}{L'_r} & 0 & -\frac{R'_r}{L'_r} & -p_p\omega_m & 0 & 0 & 0\\ 0 & L_m\frac{R'_r}{L'_r} & p_p\omega_m & -\frac{R'_r}{L'_r}0 & 0 & 0 & 0\\ -\frac{3}{2}\frac{p_p}{J_L}\frac{L_m}{L'_r}\psi_{r\beta} & \frac{3}{2}\frac{p_p}{J_L}\frac{L_m}{L'_r}\psi_{r\alpha} & 0 & 0 & 0 & -\frac{1}{J_L} & 0\\ 0 & 0 & 0 & 0 & 0 & 0 & 0\\ 0 & 0 & 0 & 0 & 0 & 0 & 0\end{bmatrix}}_{\underline{A}_{e1}} \underbrace{\begin{bmatrix}i_{s\alpha}\\ i_{s\beta}\\ \psi_{r\alpha}\\ \psi_{r\beta}\\ \omega_m\\ t_L\\ R_s\end{bmatrix}}_{\underline{x}_{e1}} + \underbrace{\begin{bmatrix}\frac{1}{L_\sigma} & 0\\ 0 & \frac{1}{L_\sigma}\\ 0 & 0\\ 0 & 0\\ 0 & 0\\ 0 & 0\\ 0 & 0\end{bmatrix}}_{\underline{B}_{e1}} \underbrace{\begin{bmatrix}v_{s\alpha}\\ v_{s\beta}\end{bmatrix}}_{\underline{u}_e} + \underline{w}_{11}(t) \qquad (3)$$

$$\underbrace{\begin{bmatrix}i_{s\alpha}\\ i_{s\beta}\end{bmatrix}}_{\underline{Z}} = \underbrace{\begin{bmatrix}1 & 0 & 0 & 0 & 0 & 0 & 0\\ 0 & 1 & 0 & 0 & 0 & 0 & 0\end{bmatrix}}_{\underline{H}_e} \begin{bmatrix}i_{s\alpha}\\ i_{s\beta}\\ \psi_{r\alpha}\\ \psi_{r\beta}\\ \omega_m\\ t_L\\ R_s\end{bmatrix} + \underline{w}_{12}(t) \qquad (4)$$

Model 2: Extended model of IM derived for the estimation of R'_r, (Model-R'_r):

$$\underbrace{\begin{bmatrix} \dot{i}_{s\alpha} \\ \dot{i}_{s\beta} \\ \dot{\psi}_{r\alpha} \\ \dot{\psi}_{r\beta} \\ \dot{\omega}_m \\ \dot{t}_L \\ \dot{R}'_r \end{bmatrix}}_{\dot{\underline{x}}_{e2}} = \underbrace{\begin{bmatrix} -\left(\frac{R_s}{L_\sigma}+\frac{L_m^2R'_r}{L_\sigma L'^2_r}\right) & 0 & \frac{L_mR'_r}{L_\sigma L'^2_r} & \frac{L_m}{L_\sigma L'_r}p_p\omega_m & 0 & 0 & 0 \\ 0 & -\left(\frac{R_s}{L_\sigma}+\frac{L_m^2R'_r}{L_\sigma L'^2_r}\right) & -\frac{L_m}{L_\sigma L'_r}p_p\omega_m & \frac{L_mR'_r}{L_\sigma L'^2_r} & 0 & 0 & 0 \\ L_m\frac{R'_r}{L'_r} & 0 & -\frac{R'_r}{L'_r} & -p_p\omega_m & 0 & 0 & 0 \\ 0 & L_m\frac{R'_r}{L'_r} & p_p\omega_m & -\frac{R'_r}{L'_r}0 & 0 & 0 & 0 \\ -\frac{3}{2}\frac{p_p}{J_L}\frac{L_m}{L'_r}\psi_{r\beta} & \frac{3}{2}\frac{p_p}{J_L}\frac{L_m}{L'_r}\psi_{r\alpha} & 0 & 0 & 0 & -\frac{1}{J_L} & 0 \\ 0 & 0 & 0 & 0 & 0 & 0 & 0 \\ 0 & 0 & 0 & 0 & 0 & 0 & 0 \end{bmatrix}}_{\underline{A}_{e2}} \underbrace{\begin{bmatrix} i_{s\alpha} \\ i_{s\beta} \\ \psi_{r\alpha} \\ \psi_{r\beta} \\ \omega_m \\ t_L \\ R'_r \end{bmatrix}}_{\underline{x}_{e2}} + \underbrace{\begin{bmatrix} \frac{1}{L_\sigma} & 0 \\ 0 & \frac{1}{L_\sigma} \\ 0 & 0 \\ 0 & 0 \\ 0 & 0 \\ 0 & 0 \\ 0 & 0 \end{bmatrix}}_{\underline{B}_{e2}} \underbrace{\begin{bmatrix} v_{s\alpha} \\ v_{s\beta} \end{bmatrix}}_{\underline{u}_e} + \underline{w}_{21}(t) \tag{5}$$

$$\underbrace{\begin{bmatrix} i_{s\alpha} \\ i_{s\beta} \end{bmatrix}}_{\underline{Z}} = \underbrace{\begin{bmatrix} 1 & 0 & 0 & 0 & 0 & 0 & 0 \\ 0 & 1 & 0 & 0 & 0 & 0 & 0 \end{bmatrix}}_{\underline{H}_e} \begin{bmatrix} i_{s\alpha} \\ i_{s\beta} \\ \psi_{r\alpha} \\ \psi_{r\beta} \\ \omega_m \\ t_L \\ R'_r \end{bmatrix} + \underline{w}_{22}(t) \tag{6}$$

Here, p_p is the number of pole pairs; $L_\sigma = \sigma L_s$ is the stator transient inductance; $\sigma = 1 - \frac{L_m^2}{L_s L'_r}$ is the leakage or coupling factor; L_s and R_s are the stator inductance and resistance, respectively; L'_r and R'_r are the rotor inductance and resistance referred to the stator side, respectively; $v_{s\alpha}$ and $v_{s\beta}$ are the stator stationary axis components of the stator voltages, respectively; $i_{s\alpha}$ and $i_{s\beta}$ are the stator stationary axis components of the stator currents, respectively; $\psi_{r\alpha}$ and $\psi_{r\beta}$ are the stator stationary axis components of the rotor flux, respectively; J_L is the total inertia of the IM and load; and ω_m is the angular velocity; As can be seen from Eqs. (3) and (4) to (5) and (6), the only difference between the two extended vectors, $\underline{x}_{e1}$ and $\underline{x}_{e2}$, are the constant states R_s and R'_r, respectively. Additionally, as in both algorithms $i_{s\alpha}$ and $i_{s\beta}$ are the measured variables, and the measurement noises, $\underline{w}_{12}$ and $\underline{w}_{22}$, are equal.

3. Development of the EKF algorithm

An EKF algorithm is developed for estimation of the states in the extended IM models given in Eqs. (2) and (3) to be used in the sensorless DVC of the IM. The Kalman filter is a well known recursive algorithm that takes the stochastic state space model of the system into account together with measured outputs to achieve the optimal estimation of states [34] in multi-input, multi-output systems. The system and measurement noises are considered to be in the form of white noise. The optimality of the state estimation is achieved with the minimization of the covariance of the estimation error. For nonlinear problems, the KF is not strictly applicable, since linearity plays an important role in its derivation and performance as an optimal filter. The EKF attempts to overcome this difficulty by using a linearized approximation where the linearization is performed about the current state estimate [35]. This process requires discretization of Eqs. (3) and (4) or (5) and (6) as below:

$$\underline{x}_{ei}(k+1) = \underline{f}_{ei}(\underline{x}_{ei}(k), \underline{u}_e(k)) + \underline{w}_{i1}(k) \tag{7}$$

$$\underline{Z}(k) = \underline{H}_e\underline{x}_{ei}(k) + \underline{w}_{i2}(k) \tag{8}$$

As mentioned before, the EKF involves a linearized approximation of the nonlinear model, Eqs. (7),(8) and uses the current estimation of states $\hat{\underline{x}}_{ei}(k)$ and inputs $\hat{\underline{u}}_e(k)$ in linearization by using

$$\underline{F}_{ei}(k) = \left.\frac{\partial \underline{f}_{ei}(\underline{x}_{ei}(k), \underline{u}_e(k))}{\partial \underline{x}_{ei}(k)}\right|_{\hat{\underline{x}}_{ei}(k), \hat{\underline{u}}_e(k)} \tag{9}$$

$$\underline{F}_{ui}(k) = \left.\frac{\partial \underline{f}_{ei}(\underline{x}_{ei}(k), \underline{u}_e(k))}{\partial u_e(k)}\right|_{\hat{\underline{x}}_{ei}(k), \hat{\underline{u}}_e(k)} \tag{10}$$

Thus, the EKF algorithm can be given in the following recursive relations:

$$\underline{N}_i(k) = \underline{F}_{ei}(k)\underline{P}_i(k)\underline{F}_{ei}(k)^T + \underline{F}_{ui}(k)\underline{D}_u\underline{F}_{ux}(k)^T + \underline{Q}_i \tag{11a}$$

$$\underline{P}_i(k+1) = \underline{N}_i(k) - \underline{N}_i(k)\underline{H}_e^T(\underline{D}_\xi + \underline{H}_e\underline{N}_i(k)\underline{H}_e^T)^{-1}\underline{H}_e\underline{N}_i(k) \tag{11b}$$

$$\hat{\underline{x}}_{ei}(k+1) = \hat{\underline{f}}_{ei}(\underline{x}_{ei}(k), \hat{\underline{u}}_e(k)) + \underline{P}_i(k+1)\underline{H}_e^T\underline{D}_\xi^{-1} \times (\underline{Z}(k) - \underline{H}_e\hat{\underline{x}}_{ei}(k)) \tag{11c}$$

Here, $\underline{Q}_i$ is the covariance matrix of the system noise, namely model error. $\underline{D}_\xi$ is the covariance matrix of the output noise, namely measurement noise. $\underline{D}_u$ is the covariance matrix of the control input noise ($v_{s\alpha}$ and $v_{s\beta}$), namely input

noise. $\underline{P}_i$ and $\underline{N}_i$ are the covariance matrix of the state estimation error and extrapolation error, respectively.

The algorithm involves two main stages: prediction and filtering. In the prediction stage, the next predicted states $\hat{\underline{f}}_{ei}(\cdot)$ and the predicted state error covariance matrices, $\underline{P}_i(\cdot)$ and $\underline{N}_i(\cdot)$ are processed, while in the filtering stage, the next estimated states, $\hat{\underline{x}}_{ei}(k+1)$, obtained as the sum of the next predicted states and the correction term (second term in Eq. (11c)) are calculated.

The schematic representation of the new EKF based switching estimation algorithm is given in Fig. 1. As can be seen in Fig. 1, two EKF algorithms with two different extended models are run consecutively, one for the estimation of R_s and one for the estimation of R'_r in this case. Thus, both algorithms estimate the same state variables except for the resistances; i.e. one of the EKFs estimates the rotor resistance during one switching period and the other estimates the stator resistance in the next switching interval and so on. After the initialization of the states and determination of t_{start} and t_{swicth}, which is the start time and duration of the EKF algorithms, respectively, the algorithms are run by switching them on and off, consecutively and for equal durations. The final values of $\underline{P}_i(k+1)$ and $\hat{\underline{x}}_{ei}(k+1)$ calculated at the end of each switching period are passed over to the next EKF algorithm at the end of the period as the initial values of the covariances and states for the new switching period during which the other algorithm will be running. The estimated resistance during the previous period is also passed on to the new algorithm and is assumed constant in the other EKF model throughout the whole switching period during which the other resistance value is calculated as well as the states variables.

4. Speed sensorless DVC system

Fig. 2 demonstrates the speed sensorless DVC system based on rotor flux. Here, $\hat{\theta}_{rf}$ stands for the position of the flux with reference to the stationary axis, while $\hat{\theta}_{rf}$ is the angular velocity of the rotating d–q axis. The velocity, field and torque controllers given in the diagram are conventional proportional-integral (PI) controllers.

5. Simulation results and observations

To test the performance of the proposed estimation method, simulations are performed on an IM with the rated parameters given in Table 1.

The values of the system parameters and covariance matrix elements are very effective on the performance of

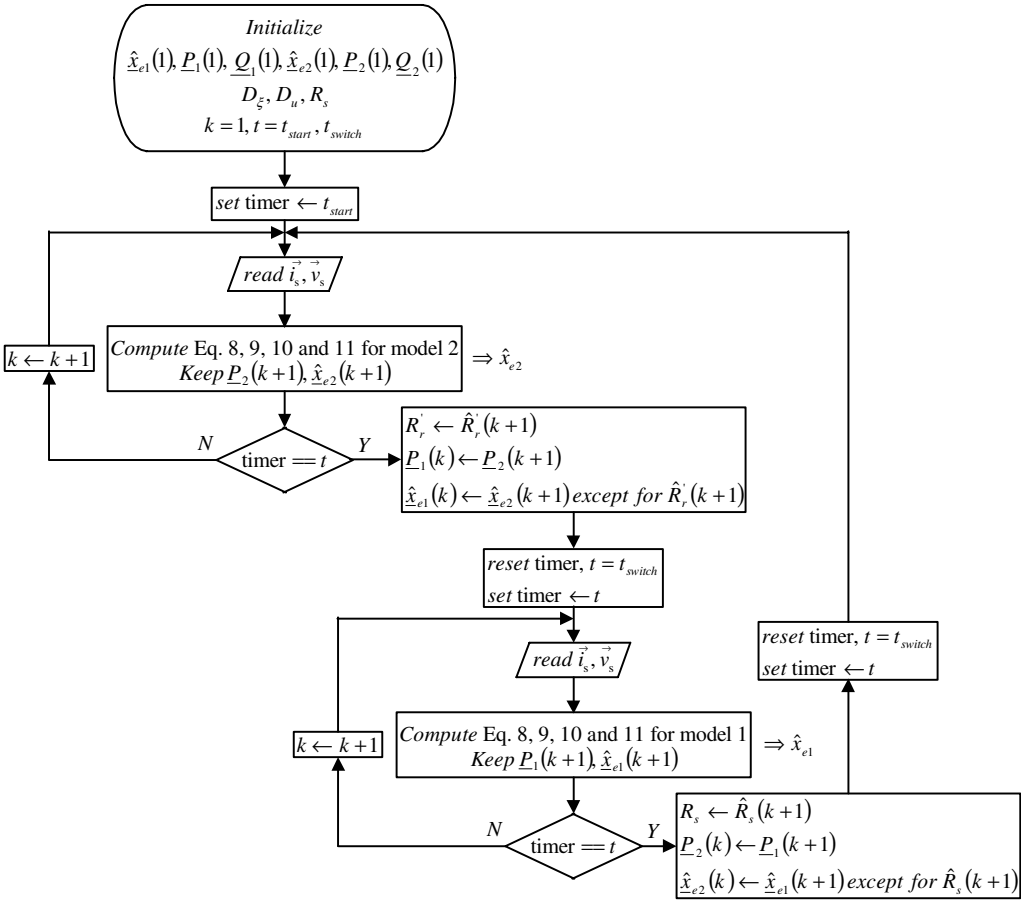

Fig. 1. Flowchart of the novel switching EKF algorithm.

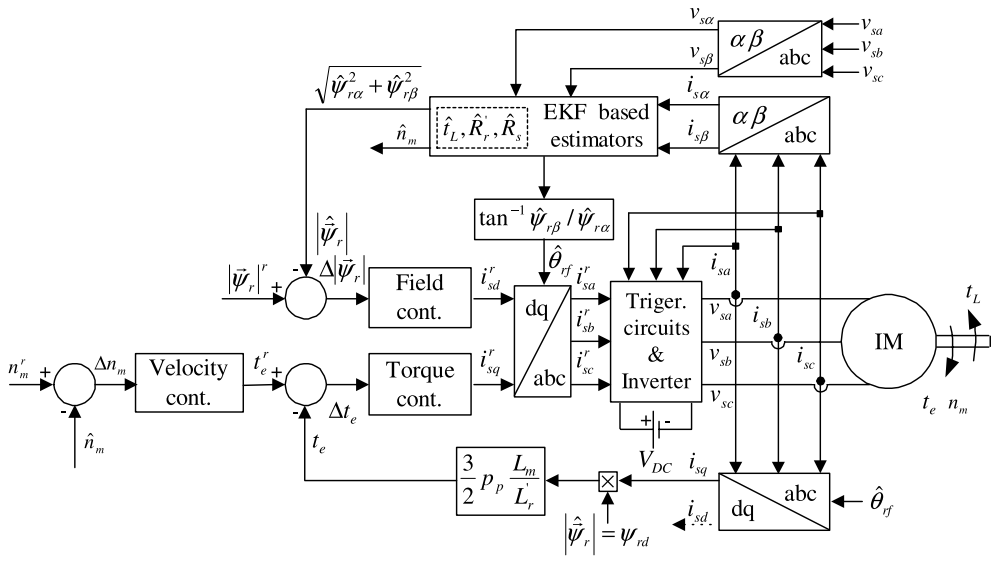

Fig. 2. Speed sensorless DVC system.

Table 1
Rated values and parameters of the induction motor used in the experiments

P (kW)	f (Hz)	J_L (kg m^2)	B_L (N m/(rad/s))	p_p	V (V)	I (A)
3	50	0.006	0.001	2	380	6.9
R_s [Ω]	R'_r[Ω]	L_s [H]	L_r [H]	L_m [H]	N_m [rpm]	T_e [N m]
2.283	2.133	0.2311	0.2311	0.22	1430	20

the EKF estimation. In this study, to avoid computational complexity, the covariance matrix of the system noise $\underline{Q}_i$ is chosen in diagonal form, which also satisfies the condition of positive definiteness. According to the KF theory, the $\underline{Q}_i$, $\underline{D}_\xi$ (measurement error covariance matrix) and $\underline{D}_u$ (input error covariance matrix) have to be obtained by considering the stochastic properties of the corresponding noises [36]. However, since these are usually not known, in most cases, the covariance matrix elements are used as weighting factors or tuning parameters. In this study, for both EKF algorithms, the tuning of the initial values of the $\underline{P}_i$ and $\underline{Q}_i$ is done by trial and error to achieve a rapid initial convergence and the desired transient and steady state behaviors of the estimated states and parameters, while the $\underline{D}_\xi$ and $\underline{D}_u$ are determined taking into account the measurement errors of the current and voltage sensors and the quantization errors of the ADCs, as given below:

For Model-R_s;

$$\underline{Q}_1 = \mathrm{diag}\{\,10^{-9}[A^2] \quad 10^{-9}[A^2] \quad 10^{-9}[Wb^2] \quad 10^{-9}[Wb^2] \quad 10^{-4}[(\mathrm{rad/s})^2] \quad 10^{-4}[(\mathrm{N\,m})^2] \quad 10^{-5}[\Omega^2]\,\}$$

$$\underline{P}_1 = \mathrm{diag}\{\,9[A^2] \quad 9[A^2] \quad 9[Wb^2] \quad 9[Wb^2] \quad 9[(\mathrm{rad/s})^2] \quad 9[(\mathrm{N\,m})^2] \quad 9[\Omega^2]\,\}$$

For Model-R'_r:

$$\underline{Q}_2 = \mathrm{diag}\{\,10^{-9}[A^2] \quad 10^{-9}[A^2] \quad 10^{-9}[Wb^2] \quad 10^{-9}[Wb^2] \quad 10^{-4}[(\mathrm{rad/s})^2] \quad 10^{-4}[(\mathrm{N\,m})^2] \quad 10^{-5}[\Omega^2]\,\}$$

$$\underline{P}_2 = \mathrm{diag}\{\,9[A^2] \quad 9[A^2] \quad 9[Wb^2] \quad 9[Wb^2] \quad 9[(\mathrm{rad/s})^2] \quad 9[(\mathrm{N\,m})^2] \quad 9[\Omega^2]\,\}$$

For both models

$$\underline{D}_\xi = \mathrm{diag}\{\,10^{-6}[A^2] \quad 10^{-6}[A^2]\,\}$$

$$\underline{D}_u = \mathrm{diag}\{\,10^{-6}[V^2] \quad 10^{-6}[V^2]\,\}$$

and sampling time $T = 100$ μs.

As can be seen from the time axis in Fig. 3, seventeen different scenarios are created to test the performance of the estimation and control algorithm in the time interval of $0 \leqslant t \leqslant 24$ s. These scenarios are developed with simultaneous changes imposed on the stator and the rotor resistance (Fig. 3a), on the velocity reference (Fig. 3b) and the load torque values (Fig. 3c) used in the simulation model.

As is well known, it is difficult to obtain the initial value of the rotor resistance in a squirrel cage IM, but that of the stator resistance can easily be determined by the DC test. Therefore, it is assumed that the initial value of the stator resistance is known at the outset of the scenarios, while the estimation of the other parameters and all the states

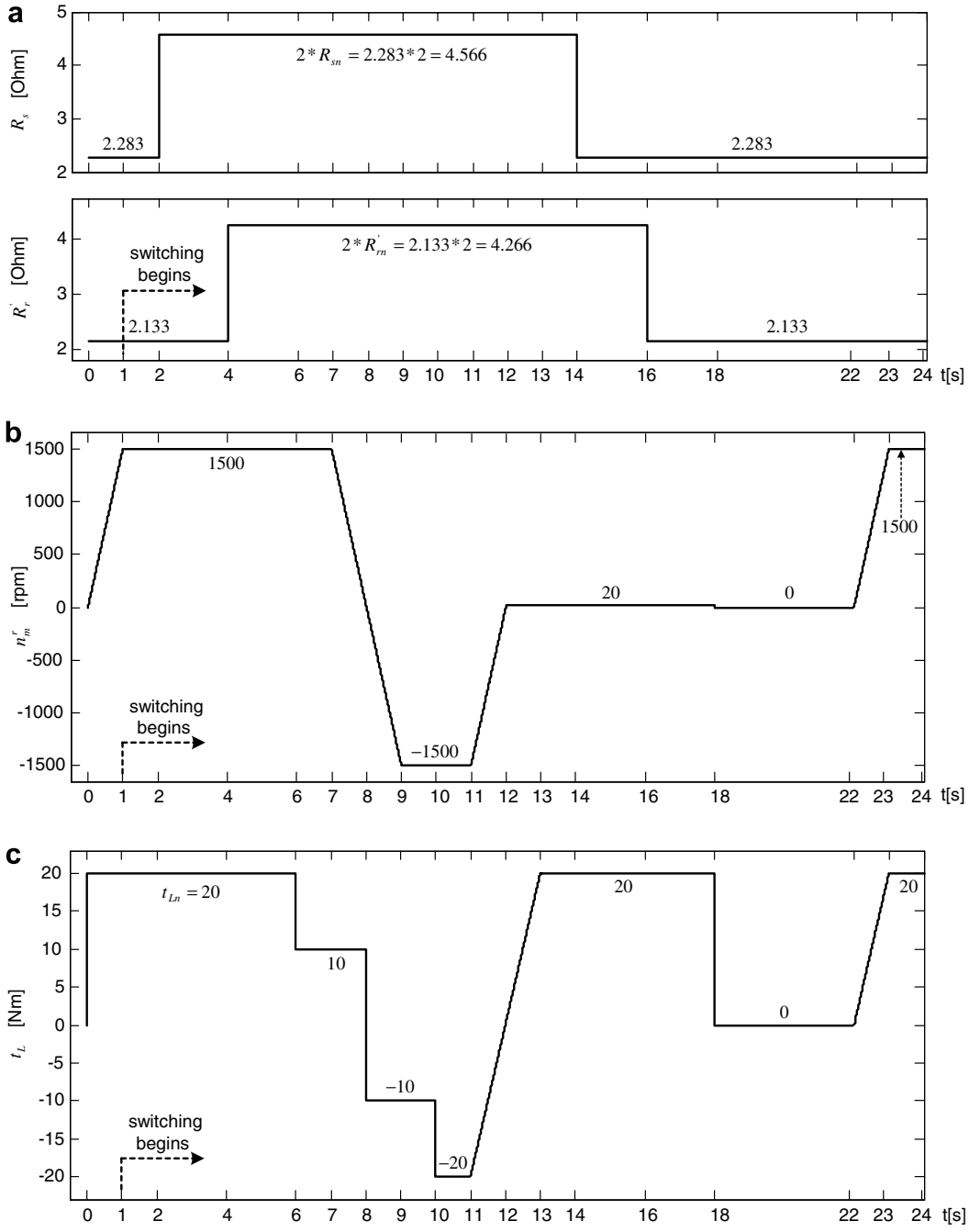

Fig. 3. Variation of the stator/rotor resistances, R_s/R_r', the reference speed value, n_m^{ref}, and applied load torque, t_L. (a) Variation of the stator/rotor resistances, R_s/R_r', (b) variation of the reference speed value, n_m^{ref} and (c) variation of the applied load torque, t_L.

is started with an initial value of zero, as a more reasonable approach. Thus, the EKF algorithm for the Model-R_r' is given a start, and after $t_{start} = 1$[s], as shown in Fig. 3, the two EKF algorithms are used consecutively by switching from one to the other at the end of a constant time interval of duration, t_{switch}, in order to estimate the rotor and stator resistances besides all the other variables required by the control scheme. For the desired transient and steady state performance criteria of this system, the t_{switch} is selected as $100 \times T$ (T is sampling period). The switching duration, t_{switch} is determined based on the following procedure:

(i) Tune $\underline{P}_i$ vs. $\underline{Q}_i$ until the desired estimation performance is achieved by each EKF algorithm; namely EKF-$\widehat{R}_s$ and EKF-$\widehat{R}_r'$.
(ii) After the tuning stage, increase $t_{switch} = n \times T$ (where $n = 1, 2, 3\ldots$ and T is sampling period) by increasing n, until the desired estimation performance is reached.

In this study, the t_{switch} is increased to $100 \times T$ in order to achieve an improved performance in the transient and steady states under *unmatched* variations of R_s and R_r', which is the most challenging case for both EKF algo-

rithms. Intervals with *unmatched* variations describe intervals during which, while one type of resistance is being estimated, the other one is given a major variation. In this study, the best "n" is also determined under unmatched variations with the following scenario, given in Fig. 3, in which EKF-$\widehat{R}'_r$ is switched *on* at $t = 2.01$ [s] when $R_s : 2 * R_{sn} \rightarrow R_{sn}$, or similarly, EKF-$\widehat{R}_s$ is switched *on* at $t = 4$[s] when $R'_r : R'_{rn} \rightarrow 2 * R'_{rn}$.

The resulting system performance for all scenarios is given with Fig. 4a representing the velocity estimate, $\hat{n}_m$, Fig. 4b depicting the velocity error, $(n_m^{ref} - \hat{n}_m)$ and Fig. 4c giving the estimation error, $n_m - \hat{n}_m$. The variation of the applied and estimated load torque is given in Fig. 5a with Fig. 5b representing the estimation error, $(t_L - \hat{t}_L)$ for this variable. The variations related to R_s are given in Fig. 6a and b with the former plot representing the actual and estimated variations of the R_s, while the latter plot represents the estimation error, $R_s - \widehat{R}_s$. As for the rotor resistance, R'_r, the actual and estimated variation of R'_r with the initial value of zero and the estimation error, $R'_r - \widehat{R}'_r$ are demonstrated with Fig. 7a and b, respectively. Finally, Fig. 8a, b and c represent the estimated flux mag-

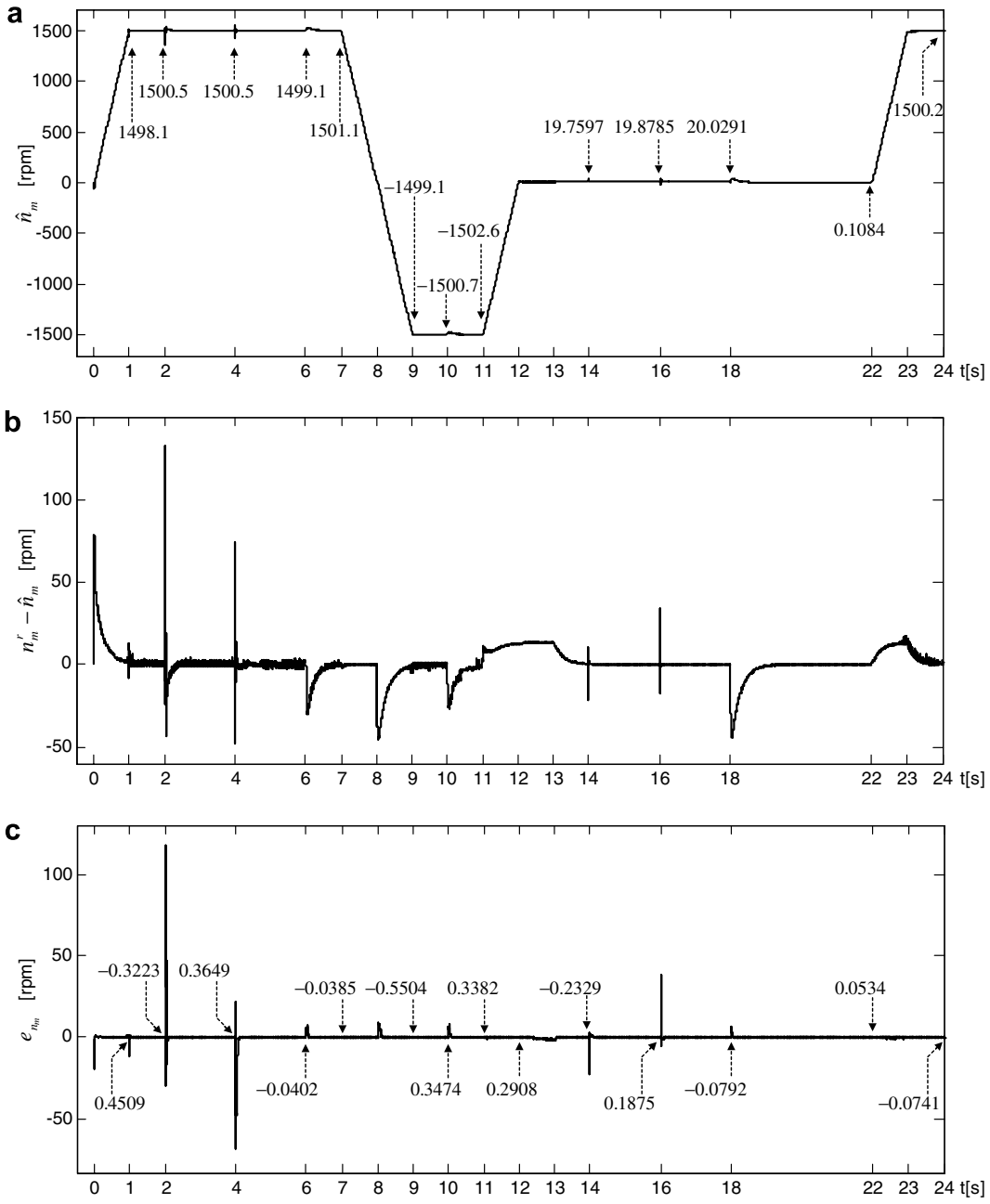

Fig. 4. Simulation results for the estimation of velocity obtained with the switching EKF estimator and DVC system. (a) Variation of the $\hat{n}_m$, (b) Variation of the velocity controller input, (c) Variation of the estimation error of $n_m, e_{n_m} = n_m - \hat{n}_m$.

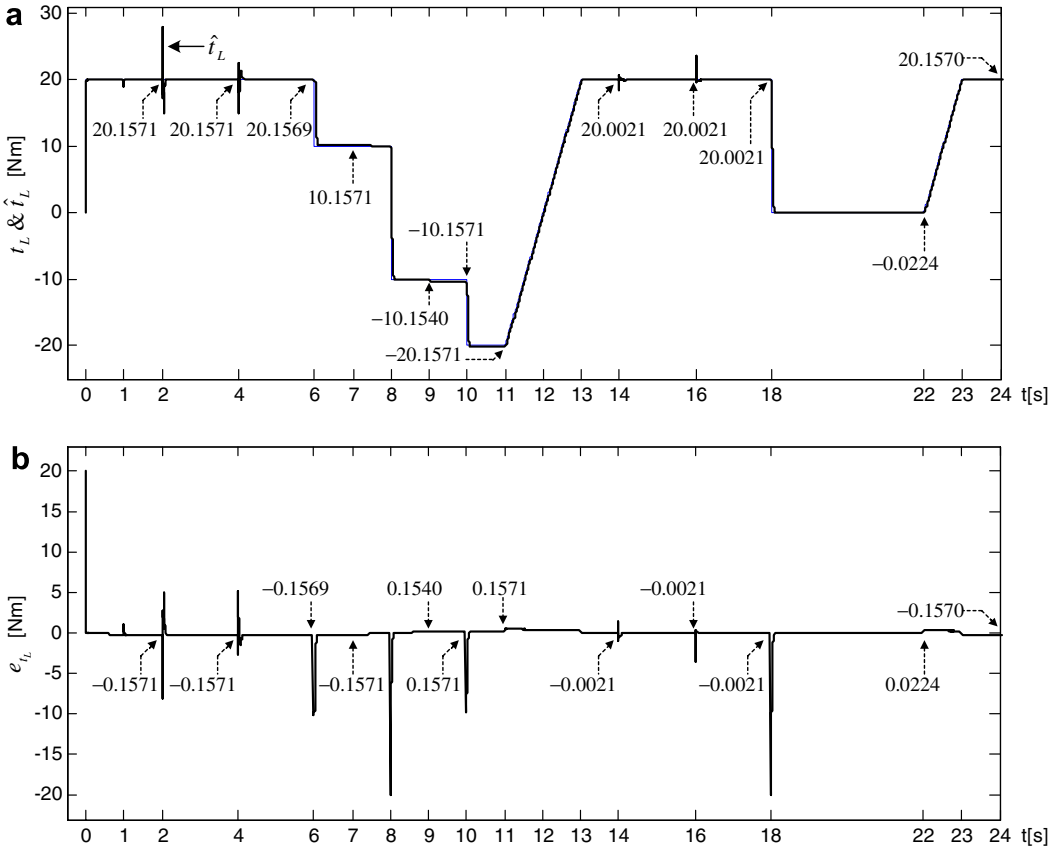

Fig. 5. Simulation results for the estimation of the load torque using the switching EKF estimator. (a) Variation of the t_L and $\hat{t}_L$, (b) Variation of the estimation error of $t_L, e_{t_L} = t_L - \hat{t}_L$.

nitude, $|\hat{\vec{\psi}}_r|$, the error between the reference and actual (estimated) flux magnitude, $|\vec{\psi}_r|^r - |\hat{\vec{\psi}}_r|$ and the flux estimation error, $(|\vec{\psi}_r| - |\hat{\vec{\psi}}_r|)$, respectively. Finally, the system performance in the zero speed range under the scenarios given in Fig. 9a is demonstrated in Fig. 9b for the estimation error, $n_m - \hat{n}_m$ and in Fig. 9c for the variation of the estimated θ_{rf}, which is the position of the flux with reference to the stator stationary axis.

Analyzing the simulation results, the following observations are made:

♦ In spite of no *a priori* information on the estimated states and parameters, except for the stator resistance initialization in the interval of 0–1[s], the estimation performances of the switching EKFs are quite good, even under challenging variations of the velocity reference and the load torque as well as matched and unmatched resistance variations.

♦ As mentioned before, the estimation and control algorithms are challenged with the unmatched variations. Even under extreme conditions, it has been demonstrated that the proposed estimation algorithm combined with the sensorless DVC performs quite well as can been seen at $t = 2.01$[s] and $t = 4$[s] under the scenarios given in Fig. 3. On the other hand, with matching algorithms and parameter variations, better transient and steady state performances are obtained with the proposed algorithm, as can be seen at $t = 14$[s] when $R_s : 2 * R_{sn} \rightarrow R_{sn}$, while R_s estimation is *on* and at $t = 16.01$[s] when $R'_r : 2 * R'_{rn} \rightarrow R'_{rn}$ while R'_r estimation is active.

♦ The new estimation technique has performed quite well also in the problematic zero speed operation [37], as can been seen in the time interval of $18[s] \leqslant t \leqslant 22[s]$ for the scenarios given in Fig. 3 and in the interval of $2[s] \leqslant t \leqslant 17[s]$ for the scenarios given in Fig. 9a. Moreover, it has been observed that the source of the estimation error of the velocity, $e_{n_m} = n_m - \hat{n}_m$, in the time interval $11[s] \leqslant t \leqslant 17[s]$ is the step shaped extreme variations of the $R'_r, R'_r : R'_{rn} \rightarrow 2 * R'_{rn}$, or $R'_r : 2 * R'_{rn} \rightarrow R'_{rn}$, which also affect the estimation of t_L, especially when $t_L = 0$ [N m] and $n_m = 0$[rpm]. However, this error also converges to *zero* as can be seen in Fig. 9b. Additionally, in the time interval $7[s] \leqslant t \leqslant 17[s]$ in Fig. 9c, which constitutes the dc condition, it can be observed that the proposed estimation technique has performed well under the most challenging operation condition inherent to the speed sensorless control of IMs.

♦ The t_L is considered constant in the EKF extended models, and the algorithm is challenged with a linear t_L variation in the time interval $11[s] \leqslant t \leqslant 13[s]$. In spite of this mismatch, satisfactory results have been obtained with the new technique.

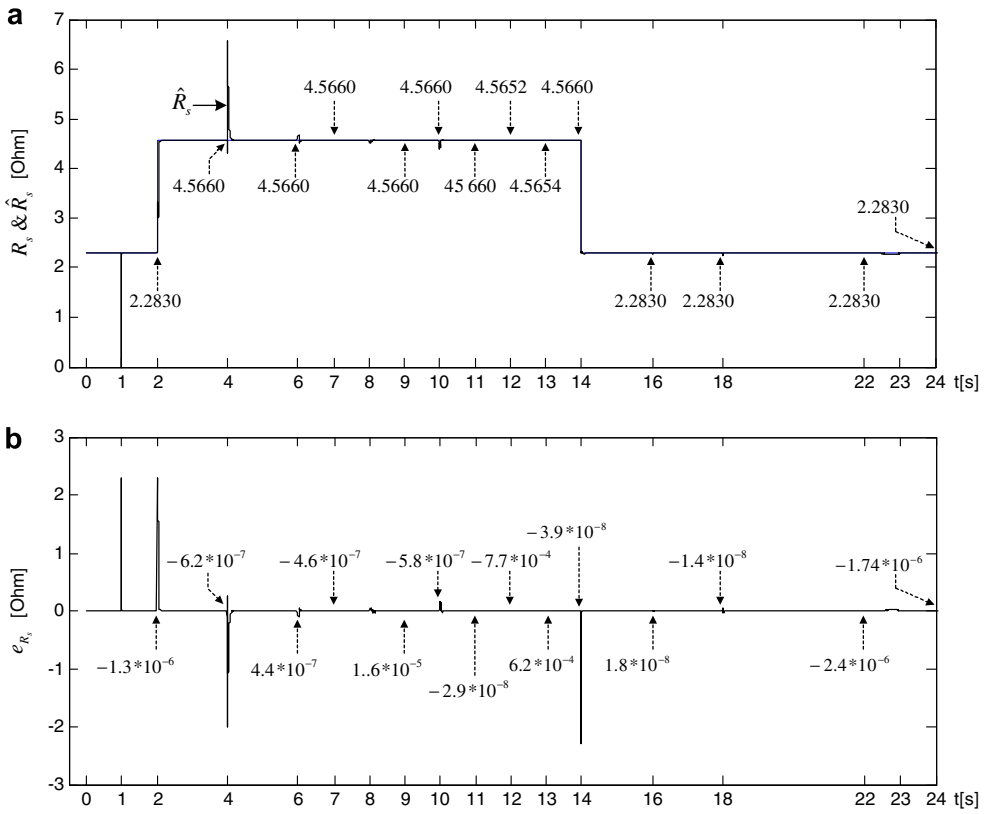

Fig. 6. Simulation results for the estimation of the stator resistance using the switching EKF estimator. (a) Variation of the R_s and $\widehat{R}_s$ and (b) variation of the estimation error of R_s, $e_{R_s} = R_s - \widehat{R}_s$.

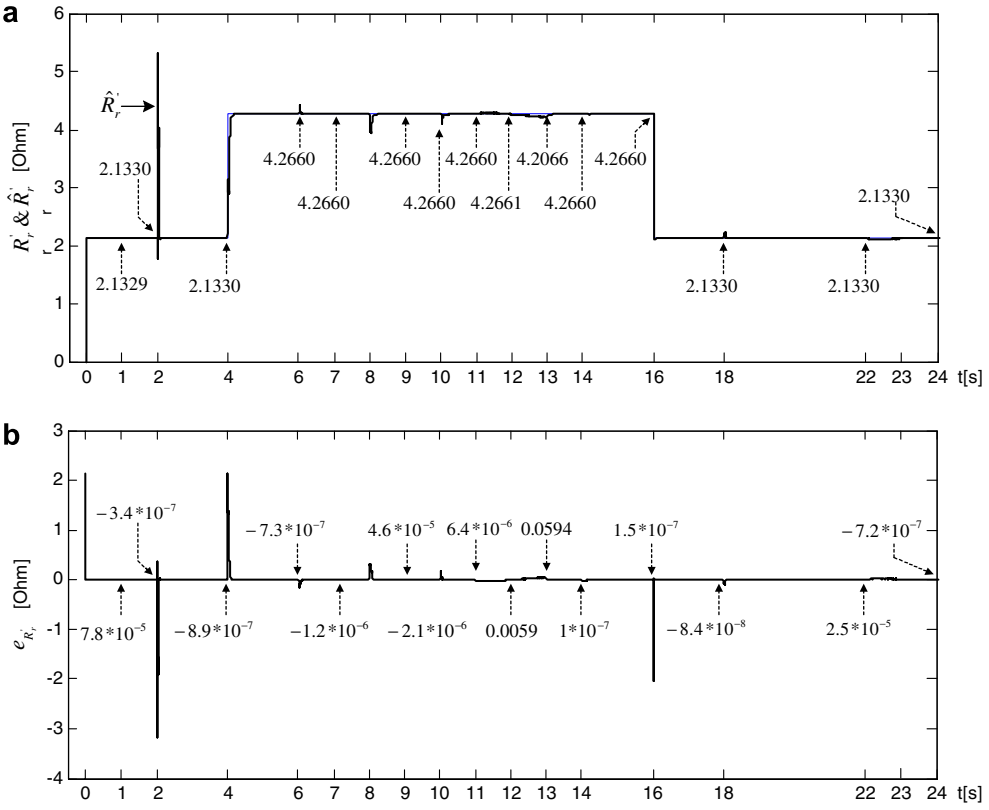

Fig. 7. Simulation results for the estimation of rotor resistance using the switching EKF estimator. (a) Variation of R_r' and $\widehat{R}_r'$ and (b) variation of the estimation error of R_r', $e_{R_r'} = R_r' - \widehat{R}_r'$.

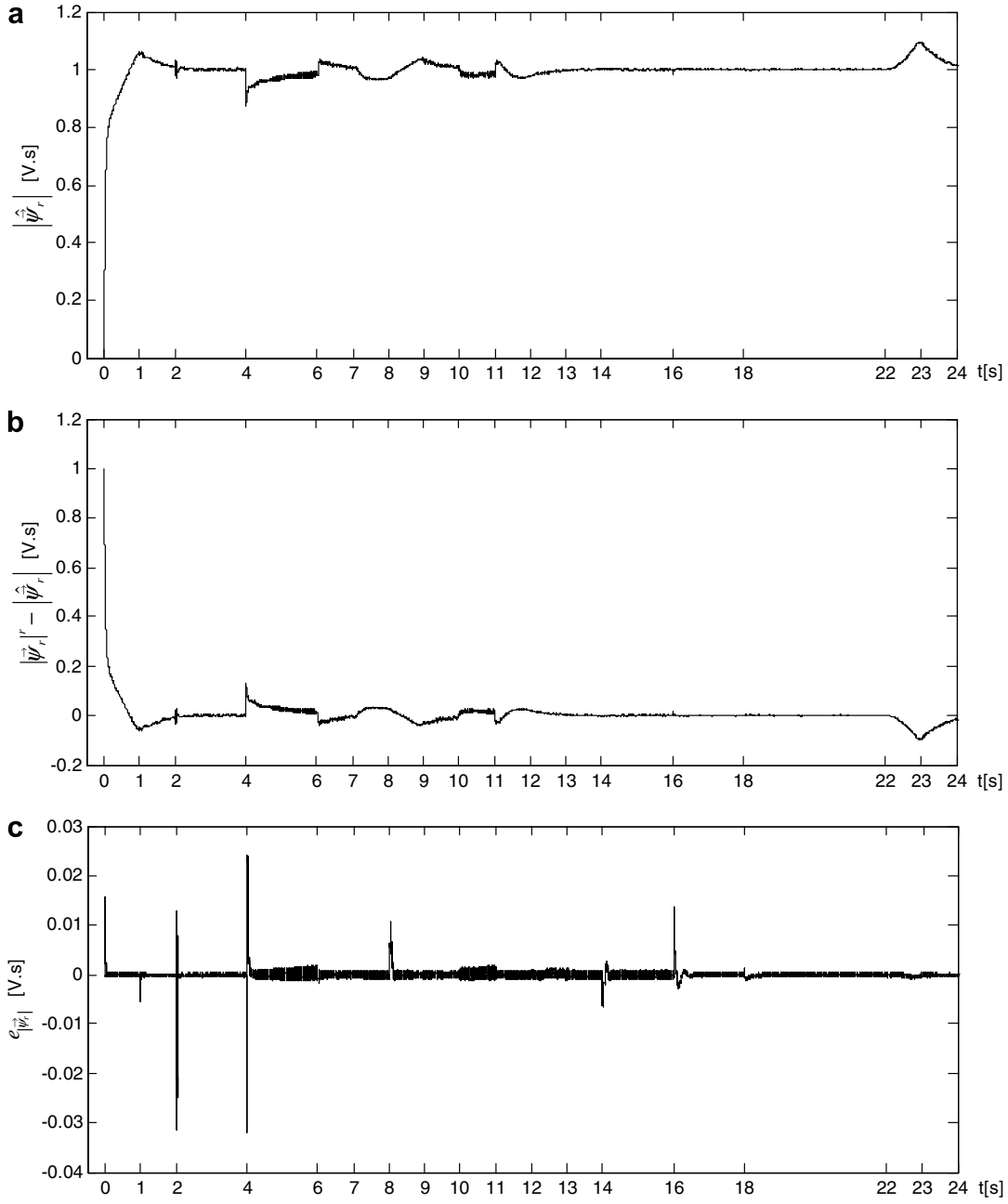

Fig. 8. Simulation results for the estimation of flux obtained with the switching EKF estimator and DVC. (a) Variation of the $|\hat{\vec{\psi}}_r|$, (b) variation of the field controller input, $\Delta|\vec{\psi}_r|$, and (c) variation of the estimation error of $|\hat{\vec{\psi}}_r|$, $e_{|\vec{\psi}_r|} = |\vec{\psi}_r| - |\hat{\vec{\psi}}_r|$.

♦ The proposed scheme also facilitates indirect evaluation of uncertainties that have the same variation as a state or parameter that is being estimated. In this study, the viscous friction ($F_v = \beta_L\, \omega_m$) is taken into account in the simulation model representing the system but not in the extended model; thus, the estimated t_L as a constant state is expected to include also the viscous friction value once the steady state is reached. This fact can be demonstrated easily as follows:

In the intervals, $1[s] \leqslant t \leqslant 7[s]$, $13[s] \leqslant t \leqslant 18[s]$ and $23[s] \leqslant t \leqslant 24[s]$, during which both the velocity reference and load torque are given positive constant values, the error in the torque estimation is $e_{t_L} \cong -0.1571$ or $e_{t_L} = -0.0021$. In the interval, $9[s] \leqslant t \leqslant 11[s]$, where both the velocity and torque reference are given negative values, the error is found to be $e_{t_L} = 0.1571$. Thus, considering the viscous friction coefficient $\beta_L = 0.001$ used in the model and the interval $1[s] \leqslant t \leqslant 2[s]$ (high speed range), the actual angular velocity is calculated as

$$\omega_m(\infty) = \hat{\omega}_m(\infty) + e_{\omega_m(\infty)} = 2\pi(1500.5 - 0.3223)/60 = 157.0982\ [\mathrm{rad/s}]$$

In the steady state, e_{t_L} should be equal to the friction taken into account in the model; hence,

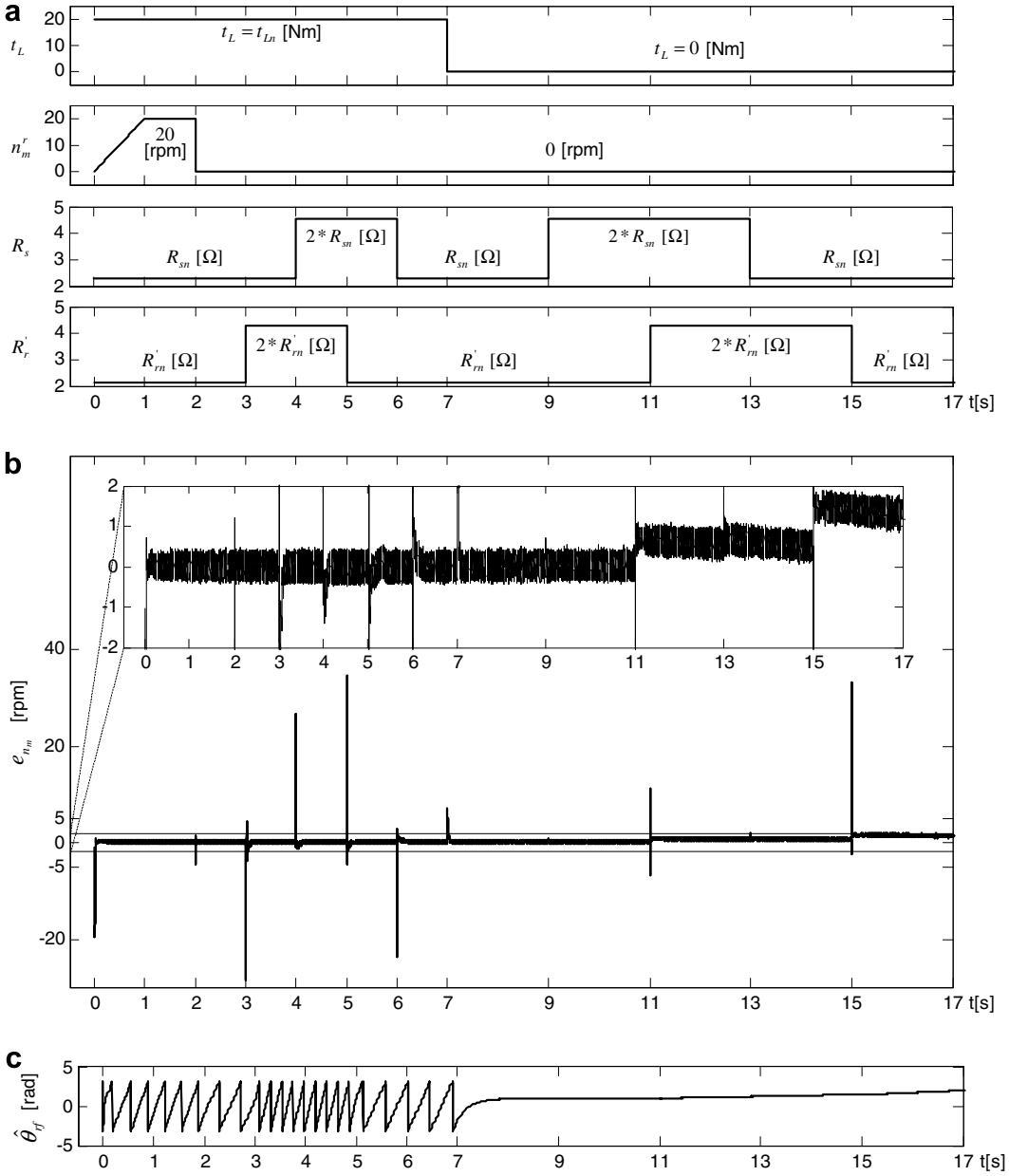

Fig. 9. Simulation results for combined switching EKF estimation and DVC for the zero speed range. (a) Variation of the applied load torque, t_L, the reference speed value, n_m^r, the stator resistance, R_s, and the rotor resistance, R'_r, for zero speed range, (b) variation of the estimation error of n_m, $e_{n_m} = n_m - \hat{n}_m$, and (c) variation of the estimated θ_{rf}.

$$e_{t_L} \stackrel{!}{=} -\beta_L \omega_m(\infty)$$
$$-0.1571 \stackrel{!}{=} -0.001 \times 157.0982$$
$$-0.1571[\text{N m}] \cong -0.1570982\ [\text{N m}] \quad (12)$$

which is almost equal to the e_{t_L} in Fig. 5(b) at $t = 2$[s].

Similar analysis can be conducted in the interval $16[\text{s}] \leqslant t \leqslant 18[\text{s}]$ (the very low speed range) during which

$$\omega_m(\infty) = \hat{\omega}_m(\infty) + e_{\omega_m(\infty)}$$
$$= 2\pi(19.8785 - 0.1875)/60 = 2.0620[\text{rad/s}] \quad (13)$$

$$e_{t_L} \stackrel{!}{=} -\beta_L \omega_m(\infty)$$
$$-0.0021 \stackrel{!}{=} -0.001 \times 2.0620 \quad (14)$$
$$-0.0021[\text{N m}] \cong -0.0020620[\text{N m}]$$

This fact should also be taken into consideration in the evaluation of the load torque estimation. By inspecting the t_L estimation, it can be observed that linear variations and reversals of t_L give rise to some estimation error for relatively short transient durations; however, in the intervals with constant velocity reference and constant t_L, this error

is much lower and almost zero once the F_v component is subtracted from t_L.

♦ Simulations are performed to compare the performance of the switching EKF algorithm with individual EKF-$\widehat{R}_s$ (with R_s estimation only) and individual EKF-$\widehat{R}'_r$ (with R'_r estimation only) for both high and low velocity operation. As can be seen in Fig. 10, two switching durations are considered for this purpose: $1 \times T$ and $100 \times T$, the latter of which gives rise to a lower estimation error, $e_{n_m} = n_m - \hat{n}_m$. As the highest velocity estimation error has occurred at the rated load torque, t_{L_n}, this value is considered in the simulation model for the comparative scenarios. Also, it is demonstrated that the initial performance of the switching operation is independent of the initial value of the R_s estimation, which is taken as 0 and R_{sn} in the simulations to demonstrate this property.

Inspection of the results demonstrates the improved performance of the new algorithms in both high and low velocity ranges. The performance deterioration of the individual EKF-$\widehat{R}_s$ and EKF-$\widehat{R}'_r$ algorithms, particularly when the speed reference approaches zero, is also obvious, as can be seen with the calculations at 6[s] based on the data given in Fig. 10a:

For $n^r_m = 1500$[rpm]

$e_{n_m}(\%)$of EKF-$\widehat{R}'_r = \frac{75.6375}{1500} \times 100 = 5.0425\%$[rpm]
$e_{n_m}(\%)$of EKF-$\widehat{R}_s = \frac{-62.4519}{1500} \times 100 = -4.1635\%$[rpm]
$e_{n_m}(\%)$of the proposed method $= \frac{0.2718}{1500} \times 100 = 0.0181\%$ [rpm]

For $n^r_m = 100$[rpm]

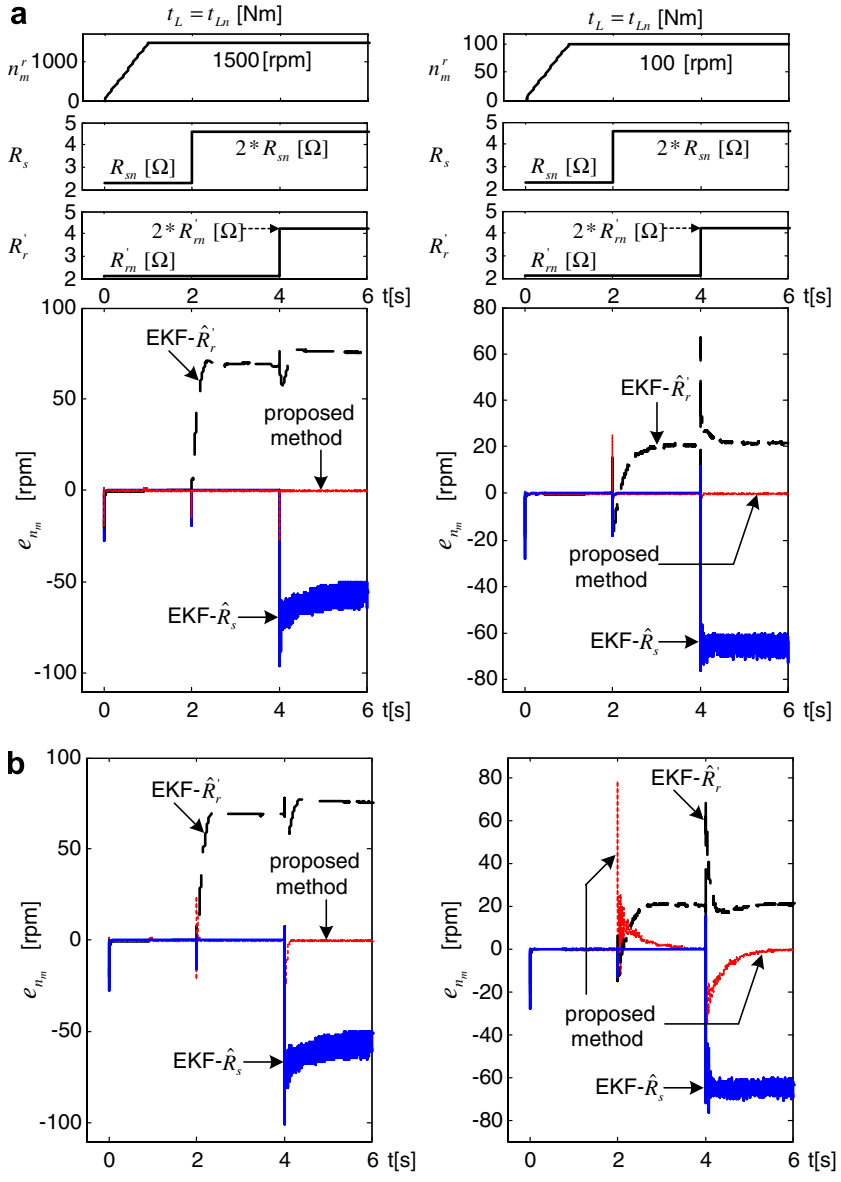

Fig. 10. Comparative results in the high and low velocity range with the EKF-$\widehat{R}_s$, EKF-$\widehat{R}'_r$ and proposed method. (a) Results with a switching duration of $100 \times T$ and (b) results with a switching duration of $1 \times T$.

$e_{n_m}(\%)$of EKF-$\widehat{R}'_r = \frac{21.5239}{100} \times 100 = 21.5239\%$[rpm]
$e_{n_m}(\%)$of EKF-$\widehat{R}_s = \frac{-64.0109}{100} \times 100 = -64.0109\%$[rpm]
$e_{n_m}(\%)$ of the proposed method $= \frac{0.1178}{100} \times 100 = 0.1178\%$ [rpm]

6. Conclusion

In this study, a switching EKF algorithm is developed for the estimation of two parameters that are critical for the high performance sensorless control of IMs, namely, R_s and R'_r. The estimation of these two parameters is often reported as a challenge in sensorless IM control. The switching algorithm developed to this aim also estimates the uncertain load torque and velocity as well as the flux and current components. In this study, the proposed algorithm is run in combination with the speed sensorless direct vector control (DVC) of IMs; however, it could be used with a variety of other methods applied for the sensorless control of IMs.

Besides the proper updates of R_s and R'_r that improve the flux and speed estimation, the performance of the switching algorithm also benefits from the estimation of velocity via the equation of motion, as opposed to its estimation as a constant as in most past studies. This approach helps restore the lost rotor information on the stator side, hence improving the very low/zero speed operation. This aspect of the study is an extension of the authors' previous research presented in Refs. [26,27].

The performance of the algorithm is tested in the very low and zero speed region and also evaluated with 17 scenarios developed by giving step type and linear variations to the load torque and angular velocity reference. The robustness of the algorithm to stator resistance, R_s, and rotor resistance, R'_r variations is tested with step type changes imposed on R_s and R'_r. As a result, the estimation of both R_s and R'_r with the new algorithm has yielded a better performance in comparison to individual EKF-$\widehat{R}_s$ and EKF-$\widehat{R}'_r$ algorithms, which conduct R_s or R'_r estimation only.

The system performance is observed to be quite good under step type variations and reversals in the load torque and step/linear changes and reversals in the angular velocity. The system has also demonstrated the expected robustness to step type variations forced on the R_s and R'_r, and acceptable errors are obtained even with the linear variations and reversals of the load torque. The estimation of the load torque, t_L, as a constant state in this algorithm, also accounts for mechanical uncertainties, which is the viscous friction torque in this case, thereby improving the estimation performance.

Finally, an important advantage of the proposed method over previous methods is that R_s and R'_r estimations can be performed both in transient and steady states without signal injection and/or algorithm changes based on parameters or speed. Other multiple model based methods, such as Refs. [28–30] are executable only during steady state and cannot handle large load torque or speed variations, as also stated by their authors. Moreover, when considering studies such as Refs. [31–33], it should be noted that adjusting the value of R'_r with respect to the estimated R_s means using only an approximate value of the actual R'_r, which does not include frequency based variations in R'_r. Thus, the proposed switching EKF method addresses all the above deficiencies by demonstrating a good performance under large uncertainties and load/speed variations in the transient and steady states.

References

[1] Ortega R, Barabanov N, Escobar G, Valderrama E. Direct torque control of induction motors: stability analysis and performance improvement. IEEE Trans Automat Control 2001;46(8):1209–22.
[2] Denaï MA, Attia SA. Intelligent control of an induction motor. Electric Power Components Syst (Taylor & Francis) 2002;30(4):409–27.
[3] Buja GS, Kazmierkowski MP. Direct torque control of PWM inverter-fed AC motors – a survey. IEEE Trans Ind Electron 2004;51(4):744–57.
[4] Takahashi I, Noguchi T. A new quick-response and high-efficiency control strategy of an induction motor. IEEE Trans Ind Appl 1986;22(5):820–7.
[5] Novotnak RT, Chiasson J, Bodson M. High-performance motion control of an induction motor with magnetic saturation. IEEE Trans Control Syst Technol 1999;7(3):315–27.
[6] Sabanovic A, Izosimov DB. Application of sliding modes to induction motor control. IEEE Trans Industry Appl 1981;IA-17(1):41–9.
[7] Wang W-J, Chen J-Y. Passivity-based sliding mode position control for induction motor drives. IEEE Trans Energy Convers 2005;20(2):316–21.
[8] Holtz J, Quan J. Drift- and parameter-compensated flux estimator for persistent zero-stator-frequency operation of sensorless-controlled induction motors. IEEE Trans Ind Appl 2003;39(4):1052–60.
[9] Lascu C, Boldea I, Blaabjerg F. Direct torque control of sensorless induction motor drives: a sliding-mode approach. IEEE Trans Industry Appl 2004;40(2):582–90.
[10] Guidi G, Umida H. A novel stator resistance estimation method for speed-sensorless induction motor drives. IEEE Trans Ind Appl 2000;36(6):1619–27.
[11] Du T, Brdys MA. Shaft speed, load torque and rotor flux estimation of induction motor drive using an extended Luenberger observer. In: Proceedings of IEEE-IEMDC'93 annual meeting, vol. 376, 1993. p.179–84.
[12] Faiz J, Sharifian MBB. Different techniques for real time estimation of an induction motor rotor resistance in sensorless direct torque control for electric vehicle. IEEE Trans Energy Convers 2001;16(1):104–9.
[13] Lin F-J. Robust speed-controlled induction motor drive using EKF and RLS estimators. IEE Proc Electric Power Appl 1996;143(3):186–92.
[14] Wade S, Dunnigan MW, Williams BW. Modeling and simulation of induction machine vector control with rotor resistance identification. IEEE Trans Power Electron 1997;12(3):495–506.
[15] Finch JW, Atkinson DJ, Acarnley PP. Full-order estimator for induction motor states and parameters. IEE Proc Electric Power Appl 1998;145(3):169–79.
[16] Wade S, Dunnigan MW, Williams BW. Comparison of stochastic and deterministic parameter identification algorithms for indirect vector control. IEE Colloq Vector Control Direct Torque Control Induction Motors 1995;2:1–5.

[17] Salvatore L, Stasi S, Tarchioni L. A New EKF-based algorithm for flux estimation in induction machines. IEEE Trans Ind Electron 1993;40(5):496–504.
[18] Bogosyan OS, Gokasan M, Hajiyev C. An application of EKF for the position control of a single link arm. In: Proceedings of IEEE-IECON'01 annual meeting, vol. 1, 2001. p. 564–9.
[19] Barut M, Bogosyan OS, Gokasan M. EKF based estimation for direct vector control of induction motors. In: Proceedings of IEEE-IECON'02 annual meeting, vol. 2, 2002. p. 1710–15.
[20] Kim Y-R, Sul S-K, Park M-H. Speed sensorless vector control of induction motor using extended Kalman filter. IEEE Trans Ind Appl 1994;30(5):1225–33.
[21] Shi KL, Chan TF, Wong YK, Ho SL. Speed estimation of an induction motor drive using an optimized extended Kalman filter. IEEE Trans Ind Electron 2002;49(1):124–33.
[22] Lee C-M, Chen C-L. Observer-based speed estimation method for sensorless vector control of induction motors. IEE Proc Control Theory Appl 1998;145(3):359–63.
[23] Wenqiang Y, Zhengchun J, Qiang X. A new algorithm for flux and speed estimation in induction machine. In: Proceedings of IEEE-ICEMS 2001 annual meeting, vol. 2, 2001. p. 698–701.
[24] Qiongxuan G, Zhiyue F. Speed estimated for vector control of induction motor using reduced-order extended Kalman filter. In: Proceedings of IEEE-PIEMC 2000 annual meeting, vol. 1, 2000. p. 138–42.
[25] El Moucary Ch, Garcia Soto G, Mendes E. Robust rotor flux, rotor resistance and speed estimation of an induction machine using the extended Kalman filter. In: Proceedings of IEEE ISIE'99 annual meeting, vol. 2, 1999. p. 742–6.
[26] Barut M, Bogosyan OS, Gokasan M. Speed sensorless direct torque control of IMs with rotor resistance estimation. Energy Convers Manage (Elsevier) 2005;46(3):335–49.
[27] Barut M, Bogosyan OS, Gokasan M. An EKF based estimator for speed sensorless vector control of induction motors. Electric Power Components Syst (Taylor & Francis) 2005;33(7):727–44.
[28] Ha I-J, Lee S-H. An online identification method for both stator-and rotor resistances of induction motors without rotational transducers. IEEE Trans Ind Electron 2000;47(4):842–53.
[29] Tajima H, Guidi G, Umida H. Consideration about problems and solutions of speed estimation method and parameter tuning for speed-sensorless vector control of induction motor drives. IEEE Trans Ind Appl 2002;38(5):1282–9.
[30] Zhen L, Xu L. Sensorless field orientation control of induction machines based on a mutual MRAS scheme. IEEE Trans Ind Electron 1998;45(5):824–31.
[31] Cirrincione M, Pucci M, Cirrincione G, Capolino G-A. An adaptive speed observer based on a new total least-squares neuron for induction machine drives. IEEE Trans Ind Appl 2006;42(1):89–104.
[32] Lascu C, Boldea I, Blaabjerg F. Very-low-speed variable-structure control of sensorless induction machine drives without signal injection. IEEE Trans Ind Appl 2005;41(2):591–8.
[33] Ohyama K, Asher GM, Sumner M. Comparative analysis of experimental performance and stability of sensorless induction motor drives. IEEE Trans Ind Electron 2005;53(1):178–86.
[34] Chen F, Dunnigan MG. Comparative study of a sliding-mode observer and Kalman filters for full state estimation in an induction machine. IEE Proc-Electric Power Appl 2002;149(1):53–64.
[35] Goodwin GC, Sin KS. Adaptive filtering prediction and control. New Jersey: Prentice-Hall Inc; 1984.
[36] Vas P. Sensorless vector and direct torque control. New York: Oxford University press; 1998.
[37] Holtz J. Sensorless control of induction motors-performance and limitations. In: Proceedings of IEEE ISIE 2000 annual meeting, vol. 2, 2000. PL12–20.